On-Line Energy Based Milling Chatter Detection

Hakan Caliskan *†

Postdoctoral Researcher,
Manufacturing Automation Laboratory
Department of Mechanical Engineering
The University of British Columbia
Vancouver, BC, Canada
Email: chakan@metu.edu.tr

Zekai Murat Kilic

Postdoctoral Researcher, Member of ASME
Manufacturing Automation Laboratory
Department of Mechanical Engineering
The University of British Columbia
Vancouver, BC, Canada
Email: zmuratk@mail.ubc.ca

Yusuf Altintas

Professor, Fellow of ASME
Manufacturing Automation Laboratory
Department of Mechanical Engineering
The University of British Columbia
Vancouver, BC, Canada
Email: altintas@mail.ubc.edu

ABSTRACT

Milling exhibits forced vibrations at tooth passing frequency and its harmonics, as well as chatter vibrations close to one of the natural modes. In addition, there are sidebands which are spread at the multiples of tooth passing frequency above and below the chatter frequency, and make the robust chatter detection difficult. This paper presents a novel on-line chatter detection method by monitoring the vibration energy. Forced vibrations are removed from the measurements in discrete time domain using a Kalman filter. After removing all periodic components, the amplitude and frequency of chatter are searched in between the two consecutive tooth passing frequency harmonics using a nonlinear energy operator. When the energy of any chatter component grows relative to the energy of forced vibrations, the presence of chatter is detected. The proposed method works in discrete real time intervals, and can detect the chatter earlier than frequency domain based methods which rely on Fast Fourier Transforms. The method has been experimentally validated in several milling tests using both microphone and accelerometer measurements, as well as using spindle speed and current signals.

Nomenclature

A Directional force coefficient matrix
F Force vector
D Lag parameter of the energy operator
ER Energy ratio
H Measurement matrix
K Kalman gain vector
K_t, K_r Cutting force coefficients
M Number of chatter frequencies and band-pass filters
N Number of spindle harmonics
N_t Number of teeth of the tool
P Error covariance matrix

---

*Instructor at Mechanical Engineering Department, Middle East Technical University, Turkey
†Address all correspondence related to ASME style format and figures to this author.

$\mathbf{Q}$ Process noise covariance matrix
R Measurement noise covariance
S_p, S_c Amplitudes of periodic and chatter harmonics
T Sampling time
$\mathbf{U}$ Mode shape matrix
a_p Axial depth of cut
c Commanded feed rate
h Chip thickness
$s(t), \hat{s}_p, s_c$ Measurement, periodic estimate, chatter component
$\mathbf{q}$ Modal displacement vector
$\mathbf{q}_k$ Kalman state vector
v Measurement noise
$\mathbf{w}$ Process noise
$\mathbf{x}, x, y$ Physical displacement
η ER integration factor
λ Process noise to measurement noise ratio
θ Angular immersion angle
τ Time delay
ϕ Phase
ω_s, ω_t Spindle, tooth passing frequency
ω_c Dominant chatter frequency
$\omega_{CH,m}$ Identified chatter frequency at m-th tooth passing interval
Φ State matrix
Ψ Nonlinear energy operator
Ω Spindle speed

1 Introduction

Stability of milling operations have been extensively studied in both frequency and discrete-time domain [1]. The stability laws require Frequency Response Function (FRF) of the machine tool and workpiece, cutting coefficients of the work material, and tool geometry. The resulting stability lobe diagrams allow the process planners to select most productive chatter free speed, depth and width of cuts on a machine tool, provided that the input data to the stability laws are accurate. However, the uncertainties in the FRF measurements and parameters, position and time varying dynamics of the machine structure and workpiece may still lead to chatter during machining. Unless avoided, chatter may damage the tool and spindle while leaving poor surface finish.

A real-time chatter identification method must continuously run during machining, detect chatter frequency, and determine a new possible chatter free spindle speed and proceed with the machining. There has been several studies to detect chatter and automatically select new spindle speed to stabilize the process. Delio et al. [2] used microphone to detect chatter frequency and update the spindle speed automatically. They removed the periodic, forced vibrations using comb filters, detected the chatter and its frequency by monitoring the Fourier spectrums of the sound measurements. Kuljanic [3] tried various sensors for chatter detection using statistical methods, and recommended that cutting torque sensing would be favorable.

Recently, sensorless methods using the CNC signals such as spindle motor current, and spindle speed have been proposed for chatter detection. Soliman et al. [4] detected chatter by monitoring the spindle motor current using statistical indicator. They measured the spindle drive's bandwidth which was about 200 Hz, and used the ratio of dynamic cutting force over static one to detect the chatter within the low frequency bandwidth of the spindle drive. Lamraoui et al. [5] monitored the instantaneous angular speed signals collected from spindle encoder. They compared the periodic and the remaining components of the speed as chatter indicator, but threshold has to be calibrated from a number of experiments. Choi et al. [6] proposed a wavelet-based maximum likelihood estimation algorithm to detect chatter from acceleration and force sensors. Tansel et. al. [7] proposed s- transformations and fuzzy logic controllers for automatic detection of chatter from acceleration sensors which need training to set-up thresholds. Similarly, articles suggest wavelet transformations with probabilistic distribution [8] and decomposition of the vibration signals [9], entropy monitoring [10, 11], and ensemble empirical mode decomposition [12–14]. These methods do not utilize the mathematical model of chatter physics, require training tests to determine thresholds, hence they are not robust for small batch manufacturing.

There are model-based predictive methods to detect chatter. vanDjik et. al [15] assigned a dynamic cutting model in discrete time domain and estimated its parameters with Normalized Least Mean Squares and Kalman filter algorithms. The onset of chatter is detected from monitoring the unstable roots of the characteristic equation of dynamic cutting system. Kuljanic et al. [16] used the moving Power Spectral Density (PSD) of cutting force and tool vibration signals and detected

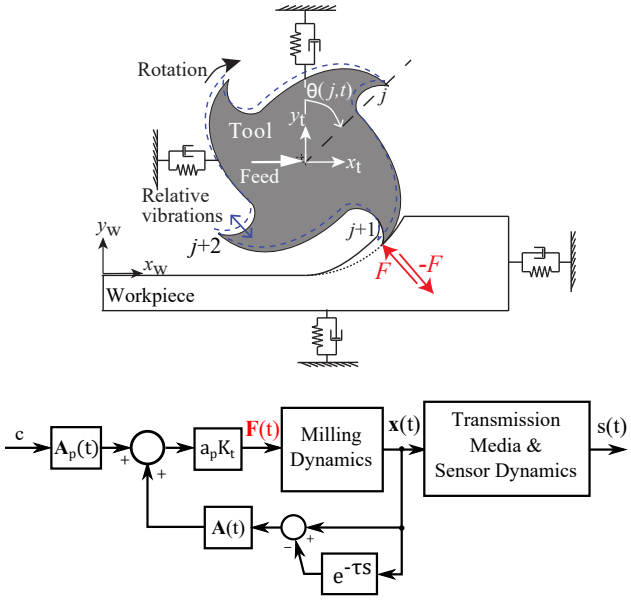

Fig. 1. Milling dynamics

the chatter using the energy ratio of the chatter component over static one. Li et al. [17] used the coherence of the two orthogonal acceleration signals to identify chatter in milling. They assumed that the tool is worn or chatter exists if the coherence approaches to unity. Hynynen et al. [18] used the coherence between the measured audio and acceleration signals to identify the chatter. Tangjitsitcharoen and Moriwaki [19] used ratio of the cutting force in different directions to detect chatter. Schmitz [20] identified chatter by using the variance of sound signals once per revolution. Similarly, Insperger et al. [21] used Poincare map shapes to characterize the forced vibrations and chatter. Kakinuma [22] developed a disturbance observer to detect chatter vibrations by using actual spindle current and speed signals. They used digital filtering for the separation of chatter and forced vibrations. These techniques have focused on the detection of chatter, which has to be accompanied by identification of chatter frequency to schedule stable spindle speed to CNC in real time. Al-Regib [23] applied Teager-Kaiser Nonlinear Energy Operator and Wigner distribution to develop a normalized chatter index using acceleration signals. They detected the chatter by checking the ratio of the energy at the high frequency band to the total energy of the signal. Fast Fourier Transform of sensor signals is the most straightforward method [24]. However there are two disadvantages: (i) FFT requires a moving time window which introduces a half period delay to the computed amplitudes of the signal, and (ii) FFT is inaccurate when handling the signal with time-varying magnitudes as shown in [25].

The existing literature either used frequency spectrum monitoring or various artificial intelligence based algorithms which require significant training. Unless the models are based on the physics of dynamic milling, it is difficult to develop a robust method to avoid false chatter detection. This paper presents the mathematical model of dynamic milling which shows the periodic components that lead to forced vibrations and regenerative terms contributed by chatter. The amplitudes and frequencies of both forced and chatter vibration components are mathematically derived (Section 2). The periodic parts are removed from the discrete time domain measurements at each sampling interval, and the chatter frequency and amplitudes are estimated using Teager-Kaiser Nonlinear Energy Operator. The presence of chatter is detected by monitoring the energy ratio between the chatter and periodic components at each sampling interval (Section 3). The proposed method has been experimentally validated with a significant number of tests, and some of them are given in the paper (Section 5). The paper is concluded with a set of recommendations in Section 6.

2 Dynamics of milling chatter

The schematics of the milling system with relative tool - workpiece vibration is shown in Fig. 1, where the subscripts t and w stand for tool and workpiece, respectively. The dynamic model of milling for process stability analysis has been presented in the past [26]. The model is extended here by including both stable and unstable solutions which are specifically used to derive the proposed chatter detection algorithm.

As shown in Fig. 1, cutting force acts at the tool and workpiece contact in the opposite directions, and it is proportional to the static and regenerative chip thickness, $h_j(t)$. For relative - tool workpiece vibrations $x(t) = x_t(t) - x_w(t)$ and $y(t) = y_t(t) - y_w(t)$ in x and y directions, the chip thickness is represented as [26]:

$$h_j(t) = c\sin\theta_j(t) + [x(t) - x(t-\tau)]\sin\theta_j(t) + [y(t) - y(t-\tau)]\cos\theta_j(t) \quad (1)$$

where the subscript j is the tooth index ($j = 1, 2 \ldots N_t$) with N_t number of teeth, and $c[mm/rev/tooth]$ is the feed rate per tooth, and $\tau[s]$ is the time delay. For a regular pitch tool rotating at spindle speed of $\Omega[rev/min]$, the delay is equal to the tooth passing period: $\tau[\mathrm{s}] = 60/\Omega N_t$. $\theta_j[rad]$ is the angular immersion angle of tooth j and is expressed as follows:

$$\theta_j(t) = 2\pi \left(\frac{\Omega}{60} t + \frac{j-1}{N_t} \right) \tag{2}$$

The tangential and radial forces for removing material with a_p depth of cut are written as [27]:

$$F_{r,j}(t) = g_j(t) \rho_j a_p K_r h_j(t) \quad ; \quad F_{t,j}(t) = g_j(t) \rho_j a_p K_t h_j(t) \tag{3}$$

~~where $g_j(t)$ is a unit step function that determines whether the j-th tooth is in or out cut~~ where $g_j(t)$ is a rectangular window function that determines whether the j-th tooth is in cut, $g_j(t) = 1$ or out of cut, $g_j(t) = 0$, and ρ_j is the run-out factor of the j-th tooth [21] . K_r and K_t are the radial and tangential cutting force coefficients, respectively. Inserting the chip thickness into tangential and radial forces, then transforming to $x-y$ frame, the dynamic force vector takes the following form:

$$\mathbf{F}(t) = \left\{ F_x(t) \; F_y(t) \right\}^T = a_p K_t \mathbf{A}(t) [\mathbf{x}(t) - \mathbf{x}(t-\tau)] + \mathbf{F}_s(t) \tag{4}$$

where the relative tool - workpiece vibration vector $\mathbf{x}(t)$ is:

$$\mathbf{x}(t) = \left\{ x(t) \; y(t) \right\}^T \tag{5}$$

The $\mathbf{A}(\mathrm{t})_{2\times 2}$ is the time varying, periodic directional force coefficient matrix [21, 27],

$$\begin{aligned}
\mathbf{A}(\mathrm{t}) &= \frac{1}{2} \times \begin{bmatrix} a_{xx}(t) & a_{xy}(t) \\ a_{yx}(t) & a_{yy}(t) \end{bmatrix} \\
a_{xx}(t) &= -\sum_{j=1}^{N_t} g_j(t) \rho_j \left[\sin 2\theta_j(t) + \frac{K_r}{K_t} \left((1 - \cos 2\theta_j(t)) \right) \right] \\
a_{xy}(t) &= -\sum_{j=1}^{N_t} g_j(t) \rho_j \left[1 + \cos 2\theta_j(t) + \frac{K_r}{K_t} \sin 2\theta_j(t) \right] \\
a_{yx}(t) &= \sum_{j=1}^{N_t} g_j(t) \rho_j \left[1 - \cos 2\theta_j(t) - \frac{K_r}{K_t} \sin 2\theta_j(t) \right] \\
a_{yy}(t) &= \sum_{j=1}^{N_t} g_j(t) \rho_j \left[\sin 2\theta_j(t) - \frac{K_r}{K_t} \left(1 + \cos 2\theta_j(t) \right) \right]
\end{aligned} \tag{6}$$

and vector $\mathbf{F}_s(t)_{2\times 1}$ includes the static cutting forces in x and y directions,

$$\mathbf{F}_s(t) = a_p K_t c \mathbf{A}_p(t) \leftarrow \mathbf{A}_p(t) = \begin{bmatrix} a_{xx}(t) \\ a_{yx}(t) \end{bmatrix} \tag{7}$$

Static cutting force $F_s(t)$ excites the system at spindle speed frequency ($\omega_s[rad/s] = 2\pi\Omega/60$) and its higher harmonics ($n\omega_s$ with index $n = 1, 2, \ldots$). The higher harmonics are due to the intermittent tool-workpiece engagement which is represented by the rectangular window function $g_j(t)$. It can be shown that the Fourier serires expansion of $g_j(t)$ consists of spindle frequency and its harmonics [28, 29]. For a tool with equal pitch spacing and zero run-out ($\rho_j = 1$), each cutting edge ($j = 1, 2, \cdots N_t$) removes the same amount of chip from the workpiece and the system becomes periodic at tooth passing frequency ($\omega_t[rad/s] = 2\pi\Omega N_t/60$) and its harmonics ($n\omega_t$ with index $n = 1, 2, \ldots$). The general case is considered in this paper, hence, the cutting force and the resulting vibrations and sound are assumed to be periodic at spindle frequency ω_s and its harmonics. ~~For a tool with zero run-out $\rho_j = 1$, each cutting edge ($j = 1, 2, \cdots N_t$) removes the same amount of chip from the workpiece and the system becomes periodic at tooth passing frequency ($\omega_t[rad/s] = 2\pi\Omega N_t/60$) and its harmonics~~

~~($n\omega_t$ with index $n = 1,2,\ldots$) . Otherwise the periodicity would be spindle speed ($\omega_s[rad/s] = 2\pi\Omega/60$) and its harmonics ($n\omega_s$ with index $n = 1,2,\ldots$) . For a general case, it is assumed that tool has radial run-outs, i.e., the directional matrix ($\mathbf{A}(t)$) coefficients and the resulting cutting forces, vibrations and sound are periodic at spindle frequency ω_s and its harmonics.~~

It is assumed that the structural dynamics of the machine system is proportionally damped. Transforming the physical relative tool-workpiece vibrations to the modal domain, $\mathbf{x}(t)_{2\times 1} = \mathbf{U}\cdot\mathbf{q}(t)$, the equation of motion takes the following form [30]:

$$\ddot{\mathbf{q}}(t) + [2\xi\omega_n]\dot{\mathbf{q}}(t) + [\omega_n^2]\mathbf{q}(t) = \mathbf{U}^T a_p K_t \mathbf{A}(t)\mathbf{U}[\mathbf{q}(t) - \mathbf{q}(t-\tau)] + \mathbf{U}^T\mathbf{F}_s(t) \tag{8}$$

where $\mathbf{U}$ is the mode shape matrix, $\mathbf{q}(t)$ is the modal displacement vector with the size of total number of vibration modes of tool and workpiece. The first term $\mathbf{F}_s(t) = a_p K_t c \mathbf{A}_p(t)$ is the quasi-static force, and regenerative part is $a_p K_t \mathbf{A}(t)\,[\mathbf{q}(t) - \mathbf{q}(t-\tau)]$ with direct $\mathbf{q}(t)$ and delayed $\mathbf{q}(t-\tau)$ vibrations, and both terms have $\mathbf{A}(t)$ and $\mathbf{A}_p(t)$ which are periodic at frequency ω_s. The solution $\mathbf{q}(t)$ of Eq. (8) is expressed by a periodic component $\mathbf{q}_p(t)$ contributed by quasi-static force and the perturbation $\mathbf{q}_c(t)$ generated by the delayed, regenerative term as follows:

$$\mathbf{q}(t) = \mathbf{q}_p(t) + \mathbf{q}_c(t) \tag{9}$$

When the system is stable with only forced vibrations, the perturbation term tends to be zero, $\mathbf{q}_c(t) = 0$. The steady state, forced vibrations become periodic at the harmonics of ω_s and can be expressed by the following ordinary differential equation (ODE):

$$\ddot{\mathbf{q}}_p(t) + [2\xi\omega_n]\dot{\mathbf{q}}_p(t) + [\omega_n^2]\mathbf{q}_p(t) = \mathbf{U}^T\mathbf{F}_s(t) \tag{10}$$

with the following particular solution:

$$\mathbf{q}_p(t) = \sum_{n=1}^{\infty} \mathbf{Q}_{p,n} e^{i(n\omega_s t)} \tag{11}$$

When the system becomes unstable, both forced and chatter vibrations occur. Subtracting the periodic ODE Eq. (10) from Eq. (8), the self excited vibrations are found from the solution of the delayed differential equation (DDE) [31], and expressed at the border of stability as:

$$\begin{aligned} \mathbf{q}_c(t) &= \mathbf{q}(t) - \mathbf{q_p}(t) \\ &= \sum_{n=-\infty}^{\infty} \left(\mathbf{Q}_{c,n} e^{i(\omega_c + n\cdot\omega_t)t} + \tilde{\mathbf{Q}}_{c,n} e^{-i(\omega_c + n\cdot\omega_t)t} \right) \end{aligned} \tag{12}$$

where the $\mathbf{Q}_{c,n}$ and $\tilde{\mathbf{Q}}_{c,n}$ are the complex coefficient vectors and their conjugates at n-th harmonic, and ω_c[rad/s] is the chatter frequency close to one of the structural modes. For the secondary Hopf bifurcation, which is the most likely case, the spectrum of vibrations will show multiple frequencies spread on the right and left of the chatter frequency (ω_c) as shown in Fig. 2. The modulations will occur at positive values of the harmonics of tooth passing frequencies, $(\pm\omega_c + n\omega_t)$ where $n = 0, \pm 1, \pm 2\ldots$. As a result, steady state solution of Eq. (8) and its transformation back to the physical domain gives the relative tool workpiece displacement vector $\mathbf{x}(t)$ as follows:

$$\mathbf{x}(t) = \sum_{n=1}^{\infty} \mathbf{X}_{p,n}\cos(n\omega_s t + \phi_{p,n}) + \sum_{n=-\infty}^{\infty} \mathbf{X}_{c,n}\cos\left((\pm\omega_c + n\omega_t)t + \phi_{c,n}\right) \tag{13}$$

where $\mathbf{X}_{p,n}$, $\mathbf{X}_{c,n}$ and $\phi_{p,n}$, $\phi_{c,n}$ are amplitude and phase vectors of the n-th periodic and chatter terms, respectively.

When a lightly damped, highly flexible thin walled workpiece chatters, the frequencies are widely spread around the dominant chatter frequency. On the other hand, when more damped machine tool structures or cutting tools chatter, the frequencies are spread less around the chatter frequency. It is assumed that chatter frequency is located between the harmonics of tooth passing frequency for a regular pitch cutter, and between the harmonics of the spindle speed for cutters

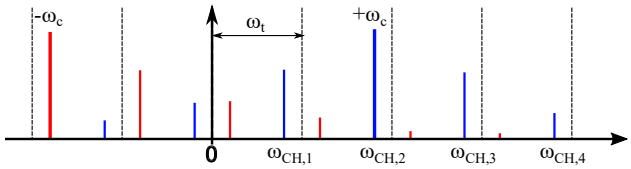

Fig. 2. Chatter frequency and its side bands

with variable pitch or run out. As shown in Fig. 2, $\omega_{CH,m}$ is defined as the m-th chatter frequency at the frequency interval $\left[(m-1)\omega_t, m\omega_t\right]$:

$$\omega_{CH} = \omega_{CH,1}, \cdots \omega_{CH,m} = \left\{\omega_c \pm n\omega_t > 0\right\} \forall n \in \mathbb{Z}^+ \tag{14}$$

Figure 1 summarizes the milling dynamics process: The commanded feedrate (c) generates forces and vibrations in $x-y$ directions, that lead to the dynamic chip thickness with a delay. The tool and workpiece vibrations are usually measured indirectly through sound, acceleration, force, spindle speed or motor current signals. Assuming a linear transfer function between the source and sensor output, the measured signal $s(t)$ has the same form of physical vibration vector $\mathbf{x}$ in Eq. (13) as:

$$s(t) = \underbrace{\sum_{n=1}^{\infty} S_{p,n}\cos(n\omega_s + \phi_{p,n})}_{s_p(t)} + \underbrace{\sum_{m=1}^{\infty} S_{c,m}\cos(\omega_{CH,m}t + \phi_{c,m})}_{s_c(t)} + v(t) \tag{15}$$

The measured vibration signals are separated into periodic forced $(s_p(t))$ and chatter $(s_c(t))$ components, and the energy content of each is evaluated. The system is assumed to chatter when the energy of the self excited term $\left\{\sum S_{c,m}\cos(\omega_{CH,m}t + \phi_{c,m})\right\}$ dominates the process.

3 Chatter Detection Model

The chatter detection strategy is shown in Fig. 3. and implemented as follows: i) the measured signal is decoupled into its forced (Eq. (11)) and unstable (Eq. (12)) components, ii) the frequencies $(\omega_{CH,m})$ and amplitude of the chatter $(S_{c,m}$, and the periodic $(S_{p,n})$ components $(n\omega_s)$ are estimated, iii) the energy contents of the periodic and chatter parts are compared. The milling system state can be measured with sensors, i.e., accelerometer, force sensor integrated to the spindle, or a microphone attached to the machine tool. The sensor signal is passed from a Kalman filter to extract the amplitudes at the frequency (ω_s) of the periodic milling system and its harmonics (i.e., $S_{p,n}$ in Eq. (15)). Then, the unstable component of the vibration ($s_c(t)$ in Eq. (15)) is obtained by subtracting the periodic component $(s_p(t))$ from the measured state $(s(t))$. The chatter-prone frequencies are located not at the harmonics of forced vibration frequency but in between them, where a weak vibration mode is present. A bank of M-bandpass filters is used to isolate any frequency that lies outside two harmonics of forced vibration frequencies, i.e., $\left[(m-1)\omega_t, m\omega_t\right]$ extending up to the highest possible natural frequency of the machining system (i.e., 5 kHz). The filtered signals are dominated by chatter $(S_{c,m})$ if it is present. The dominant chatter frequency (ω_{CH}) and its amplitude are computed at each time interval in between the harmonics of ω_t. The energies of forced and chatter prone vibrations are compared. Chatter is detected if the energy of unstable frequency component is more than the energies at forced vibration frequencies $(n\omega_s : n = 1, 2, \cdots)$. The entire algorithm is in discrete time domain and executed at sampling time interval $T[\mathrm{s}]$ which is typically about $50[\mu\mathrm{s}]$ to cover vibrations up to about 10 kHz.

3.1 Estimation of Periodic Signal

The periodic part of a measured signal is created by the forced vibrations (Eq. (13)) and is expressed with N harmonics in discrete time domain as:

$$s_p(t_k) \cong \sum_{n=1}^{N} S_{p,n}(t_k)\cos(n\omega_s t_k + \phi_{p,n}) \tag{16}$$

where $S_{p,n}(t_k)$ is the amplitude of the $n-$th spindle harmonic $(n = 1, 2...N)$ with frequency $n\omega_s$ at discrete time step $t_k = kT$. For notational convenience the sampling time, T, is omitted and the discrete time varying quantities are represented by

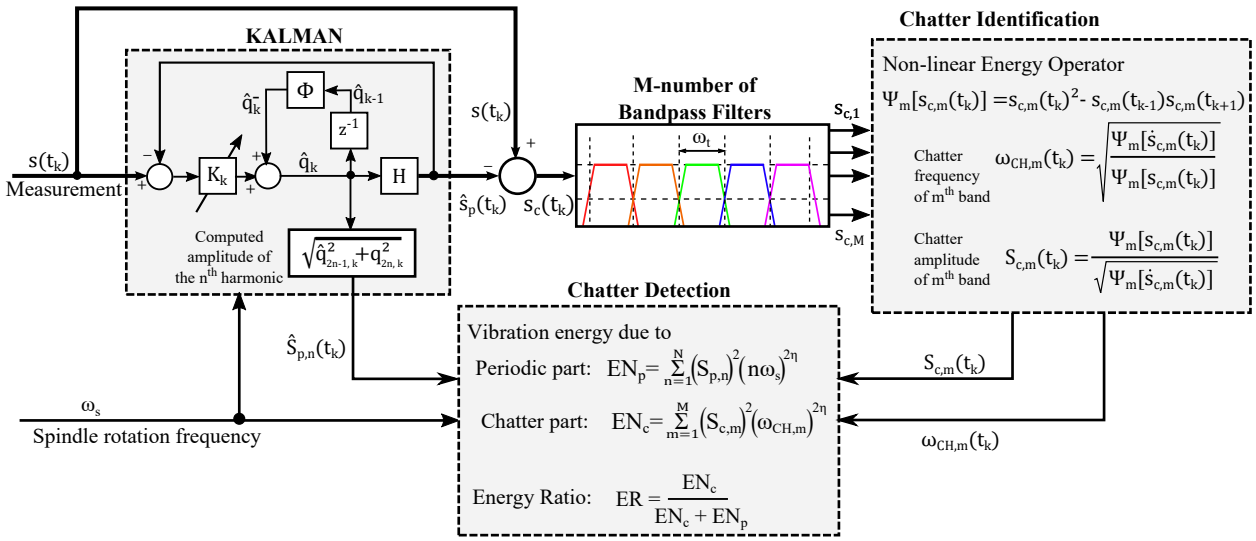

Fig. 3. Proposed methodology

subscript k only. Since the DDE of Eq. (10) is solved at the stability border, the periodic component $s_p(t_k)$ in Eq. (15) is represented by constant amplitude harmonics. However, outside the stability border, the second component of Eq. (15) will have exponentially increasing vibration amplitudes resulting in time-varying force harmonics. Therefore, in Eq. (16) the periodic component $s_p(t_k)$ is modeled with time varying amplitudes. The state variable representation of Eq. (16) with N-number of spindle harmonics is expressed as follows:

$$\underbrace{\begin{bmatrix} q_1 \\ q_2 \\ \vdots \\ q_{2N} \end{bmatrix}_{k+1}}_{\mathbf{q}_{k+1_{2N\times 1}}} = \underbrace{\begin{bmatrix} \Phi_1 & 0 & \cdots & 0 \\ 0 & \Phi_2 & \cdots & 0 \\ \vdots & & \ddots & \vdots \\ 0 & \cdots & & \Phi_N \end{bmatrix}}_{\Phi_{2N\times 2N}} \underbrace{\begin{bmatrix} q_1 \\ q_2 \\ \vdots \\ q_{2N} \end{bmatrix}_{k}}_{\mathbf{q}_{k_{2N\times 1}}} + \underbrace{\begin{bmatrix} w_1 \\ w_2 \\ \vdots \\ w_{2N} \end{bmatrix}_{k}}_{\mathbf{w}_{k_{2N\times 1}}} \tag{17}$$

$$s(t_k) = \underbrace{\begin{bmatrix} 1 & 0 & \cdots & 1 & 0 \end{bmatrix}}_{\mathbf{H}_{1\times 2N}} \begin{bmatrix} q_1 \\ q_2 \\ \vdots \\ q_{2N-1} \\ q_{2N} \end{bmatrix}_k + v_k \tag{18}$$

where, Φ_n with $(n = 1, 2 \cdots N)$ is the state transition matrix used to model the n-th harmonic. Its derivation is given in Appendix A, and it is defined as

$$\Phi_n = \begin{bmatrix} \cos(n\omega_s T) & -\sin(n\omega_s T) \\ \sin(n\omega_s T) & \cos(n\omega_s T) \end{bmatrix} \tag{19}$$

The state vector $\mathbf{q}_k$ of the periodic signal (Eq. (17)) is estimated with the following Kalman filter [32]:

$$\left.\begin{aligned} \hat{\mathbf{q}}_k^- &= \Phi \hat{\mathbf{q}}_{k-1} \\ \mathbf{P}_k^- &= \Phi \mathbf{P}_{k-1} \Phi^T + \mathbf{Q} \\ \mathbf{K}_k &= \mathbf{P}_k^- \mathbf{H}^T \left(\mathbf{H}\mathbf{P}_k^- \mathbf{H}^T + R\right)^{-1} \\ \hat{\mathbf{q}}_k &= \hat{\mathbf{q}}_k^- + \mathbf{K}_k \left(s_k - \mathbf{H}\hat{\mathbf{q}}_k^-\right) \\ \mathbf{P}_k &= (\mathbf{I} - \mathbf{K}_k \mathbf{H}) \mathbf{P}_k^- \end{aligned}\right\} \tag{20}$$

where $\hat{\mathbf{q}}_k$ is the $2N \times 1$ estimated state vector, $\mathbf{P}_k$ is the $2N \times 2N$ error covariance matrix and the superscript $(\cdot)^-$ denotes prior estimate. $\mathbf{K}_k$ is the recursively updated $2N \times 1$ Kalman gain matrix. $\mathbf{Q} = Q\mathbf{I} = E[\mathbf{w}\mathbf{w}^T]$ is the $2N \times 2N$ diagonal process noise covariance matrix, and R is the covariance of the measurement noise $E[vv^T]$, where $E[\cdot]$ is the expectation operator. R

is found by taking the covariance of measured air cutting signal, and the process noise covariance is assumed to be $Q = \lambda R$ where λ is tuned as $\lambda = 10^{-6}$

The periodic part of the measured signal is estimated as:

$$\hat{s}_p(t_k) = \mathbf{H}\hat{\mathbf{q}}_k \tag{21}$$

and subtracting it from the measured signal the chatter part is found and is expressed in discrete time with $M-$number of harmonics as:

$$\begin{aligned} s_c(t_k) &= s(t_k) - \hat{s}_p(t_k) \\ &\cong \sum_{m=1}^{M} S_{c,m}(t_k)\sin(\omega_{CH,m}t_k + \phi_{c,m}) \end{aligned} \tag{22}$$

3.2 Reconstructing the Chatter Component

Nonlinear Energy Operator (NEO) was developed by Teager and introduced by Kaiser [33], it is defined as:

$$\Psi\big[s(t)\big] = \dot{s}(t)^2 - s(t)\ddot{s}(t) \tag{23}$$

For a sinusoidal signal $s(t)$ with amplitude A and frequency ω, the NEO outputs $\Psi\big[s(t)\big] = A^2\omega^2$. Similarly, the NEO can be applied to the derivative of the signal as $\Psi\big[\dot{s}(t)\big] = (A\omega)^2\omega^2$. Based on the fact that $\omega^2 = \Psi[\dot{s}(t)]/\Psi[s(t)]$ and $A = \Psi[s(t)]/\sqrt{\Psi[\dot{s}(t)]}$, Maragos et. al. [34] developed the Energy Separation Algorithm (ESA) for estimating the time varying amplitude and instantaneous frequency of a real valued signal. The derivation of NEO and ESA with its discretization is given in Appendix B.

The chatter frequencies $\omega_{CH,m}(t_k)$ and their amplitudes $S_{c,m}(t_k)$ are found by ESA algorithm. The chatter part of the signal $s_c(t_k)$ is filtered through a bank of band passfilters in order to isolate each individual chatter frequency $\omega_{CH,m}$. According to Eq. (14), the band interval is set as tooth passing frequency. As shown in Fig. 3, each bandpass filter removes all frequencies except the band $(m-1)\omega_t < \omega_{CH,m} < m\omega_t \rightarrow m = 1,2,..,M$, hence M-number of bandpass filters are needed to search the chatter frequency $\omega_{CH,m}$. In most common milling operations, chatter occurs within 5 kHz, hence $\omega_t M \leq 5000$ Hz.

The chatter frequency and amplitude in each individual m-th band are identified in real time via ESA algorithm as follows:

$$\begin{aligned} \omega_{CH,m}(t_k) &= \arccos\left(1 - \frac{\Psi_d[y_{k-2D}] + \Psi_d[y_{k-D}]}{4\Psi_d[s_{c,m}(t_{k-2D})]}\right) \\ |\, S_{c,m}(t_k))\,| &= \sqrt{\frac{\Psi_d[s_{c,m}(t_{k-2D})]}{1 - \left(1 - \frac{\Psi_d[y_{k-2D}] + \Psi_d[y_{k-D}]}{4\Psi_d[s_{c,m}(t_{k-2D})]}\right)^2}} \end{aligned} \tag{24}$$

where Ψ_d terms are the generalized discrete form of the NEO:

$$\left.\begin{aligned} \Psi\big[y_{k-D}\big] &= \frac{1}{T^2}\left(y_{k-D}^2 - y_{k-2D}\cdot y_k\right) \\ \Psi\big[y_{k-2D}\big] &= \frac{1}{T^2}\left(y_{k-2D}^2 - y_{k-3D}\cdot y_{k-D}\right) \end{aligned}\right\} \tag{25}$$

with the following difference operators

$$\left.\begin{aligned} y_{k-D} &= s_{c,m}(t_{k-D}) - s_{c,m}(t_{k-2D}) \\ y_{k-2D} &= s_{c,m}(t_{k-2D}) - s_{c,m}(t_{k-3D}) \\ y_{k-3D} &= s_{c,m}(t_{k-3D}) - s_{c,m}(t_{k-4D}) \end{aligned}\right\} \tag{26}$$

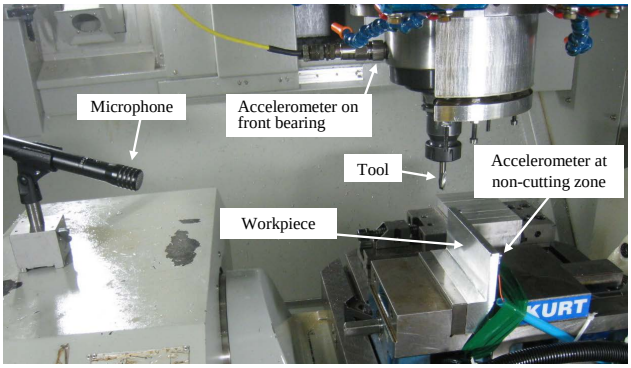

Fig. 4. Experimental setup.

and with lag parameter D which was introduced by Lin et. al. [35] in order to optimize the signal to noise ratio of the NEO. Here, the lag parameter is set equal to the time distance between the peak and zero of a sinusoidal wave, i.e., one quarter of the corresponding m-th chatter frequency. Since $\omega_{CH,m}$ is not known, median frequency of the m-th band is used in the calculation of lag parameter D as follows:

$$D = \text{round}\left(\frac{1}{4T}\frac{2\pi}{(m-0.5)\omega_t}\right) \tag{27}$$

The chatter amplitudes and frequencies are identified with $2D$ samples delay.

3.3 Energy ratio as chatter indicator

Chatter can be detected by predicting the energy content of the tool workpiece displacements. A measured velocity or acceleration signal can be directly integrated and converted into displacement as well. The product of the amplitude and frequency of the converted signal is used as a measure of vibration energy. Hence the ratio of the energy of the chatter component to the total vibration energy is used as the chatter indicator. The non-dimensional energy ratio ER is defined as follows,

$$ER = \frac{\sum_{m=1}^{M} S_{c,m}^2 \left(\omega_{CH,m}\right)^{2\eta}}{\sum_{n=1}^{N} \hat{S}_{p,n}^2 \left(n\omega_s\right)^{2\eta} + \sum_{m=1}^{M} S_{c,m}^2 \left(\omega_{CH,m}\right)^{2\eta}} \tag{28}$$

where the numerator is the energy of the chatter component, and the first term of the denominator is the energy due to periodic forcing component. The integration factor η is determined by the type of the measured signal. For measured displacement signal, $\eta = 1$, whereas for velocity and acceleration signals, $\eta = 0$ and $\eta = -1$, respectively. For microphone, $\eta = 0$ since the measured sound pressure signal is related to the velocity of vibrations at the source [36]. The amplitude of the n-th spindle harmonic is found by using the trigonometric identity $cos^2(\omega t_k) + sin^2(\omega t_k) = 1$ as follows:

$$\hat{S}_{p,n}(t_k) = \sqrt{\hat{q}_{2n-1,k}^2 + \hat{q}_{2n,k}^2} \tag{29}$$

4 Experimental Validation

The proposed chatter detection method has been verified in milling tests with flexible tools and workpieces. Although a significant amount of tests have been carried out using spindle motor current, cutting force, spindle velocity also, only sound and acceleration signals are presented since they are most practical to be used in industry. Three test cases with different tools and cutting conditions are selected to demonstrate the proposed method. In the first test case, a flexible workpiece was machined to assess the performance of the Kalman filter, energy separation algorithm and the energy ratio as a chatter indicator. Second test case was under stable and chatter conditions dominated by the flexibility of end mill. Third test is for the comparison of energy ratio indicators from sound and acceleration sensors. The parameters of the Kalman and bandpass filters for all three cases are summarized in Table 1. The general experimental setup is shown in Fig. 4.

Case 1: Milling a flexible, thin walled aluminum workpiece with a 10 mm diameter two fluted end mill

Table 1. Parameters of the algorithm

		Kalman Parameters		Bandpass	
	ω_s [Hz]	N	λ, R	M	Order
Case 1	200	26	$\lambda = 10^{-6}$	12	4
Acc.			$R = 39.16$		
Mic.			$R = 1.93^{-5}$		
Case 2	166.7	20	$\lambda = 10^{-4}$	4	4
Mic.			$R = 1.63.10^{-1}$		
Mic.			$R = 2.68.10^{-2}$		
Case 3	150	32	$\lambda = 10^{-6}$	15	4
Mic.			$R = 1.94.10^{-7}$		
Acc.			$R = 1.95.10^{-2}$		
			$\lambda = 10^{-5}$		
Speed			$R = 1.03.10^{-4}$		
Current			$R = 1.04.10^{-3}$		

A thin walled Aluminum Al7050-T7451 workpiece with $5 \times 50 \times 107$ mm dimensions is clamped to the vise. A Dtran 3225 F1 accelerometer with 10[mV/g] sensitivity is attached to the workpiece at the cutting-free side of the wall, and a microphone is placed in the enclosed area of the five axis Quaser UX600 CNC machining center. CUTPRO MALDAQ$^{(\mathbf{TM})}$ data acquisition system has been used to collect the vibration and sound data at 25600 Hz sampling frequency.

The process was down milling with a constant axial depth of cut of 14 mm. The radial immersion was increased from 1.5 to 3 mm linearly to have both stable and unstable zones in one cutting test. When the radial immersion reached at a critical value, the transition from stable to chatter can be observed. The measured acceleration signals are shown in Fig. 5.a, where chatter seems to start at about $t = 2.4s$. Cutting conditions are given in the caption of Fig. 5. The tool is assumed rigid when compared with the flexible thin wall workpiece, whose first 3 natural frequencies are identified through impulse hammer test as 1557 Hz, 2180 Hz and 3948 Hz before the cutting, and as 1852 Hz, 2434 Hz, 4039 Hz after the cutting.

Performance of periodic component estimation via Kalman algorithm: The estimation of periodic component via Kalman algorithm is illustrated using the acceleration measurements as shown in Fig. 5. The cutter has two flutes and the spindle speed is 12000 rev/min (or $\omega_s = 200$ Hz), which corresponds to tooth passing frequency of 400 Hz. By considering tool run out, $N = 26$ spindle harmonics are used in Kalman filter covering chatter frequency range up to $N\omega_s = 5200$ Hz. The estimated periodic components of the acceleration signal is superimposed on both stable and unstable measurements in Fig. 5.b. When the process is stable, the estimated periodic components match with measurements. When the process is unstable, the periodic components have less amplitude than the measurements, which are clearly evident in both time and frequency domain results shown in Fig. 5.b and c. When the estimated periodic parts are subtracted from the stable measurements (Eq. (22)), the spectrum of the stable cutting zone has no strength left except a little at the chatter prone frequency. However, when the process is unstable, the spectrum is dominated only by the chatter at the frequencies $\omega_{CH,m}$ with $m = 5 \cdots 10$ as shown in Fig. 5.d.

A bank of $M = 14$ Butterworth 4-th order band-pass filters covering the frequency range from 400 Hz to 5200 Hz are used to detect the chatter frequencies (Fig. 6). The band-stop frequencies of each filter intersect at tooth passing frequency harmonics of 400 Hz with -3 dB magnitude.

Performance of chatter frequency and amplitude estimation via ESA algorithm: The performance of chatter frequency and amplitude estimation via ESA is illustrated on the experimental results as shown in Fig. 7. After the periodic forced vibrations are removed from the measurements (Eq. (22)), the remaining data contains only chatter components as given in Fig. 7.a. Chatter appears to start at around time $t = 2.4$[s]. The tracked chatter frequencies ($\omega_{CH,m}$) and the corresponding amplitudes are shown in Fig. 7.b. Only four frequency bands ($m\omega_t$; $m = 5-8$;) where chatter appears to be present, are shown for the clarity. As seen in Fig. 7.b, in the beginning of chatter vibrations, $t = 2.50 - 2.55$[s], the dominant frequencies are at $\omega_{CH,6} = 2330$ Hz and $\omega_{CH,7} = 2769$ Hz with average amplitudes of 100[m/s^2]. The predicted

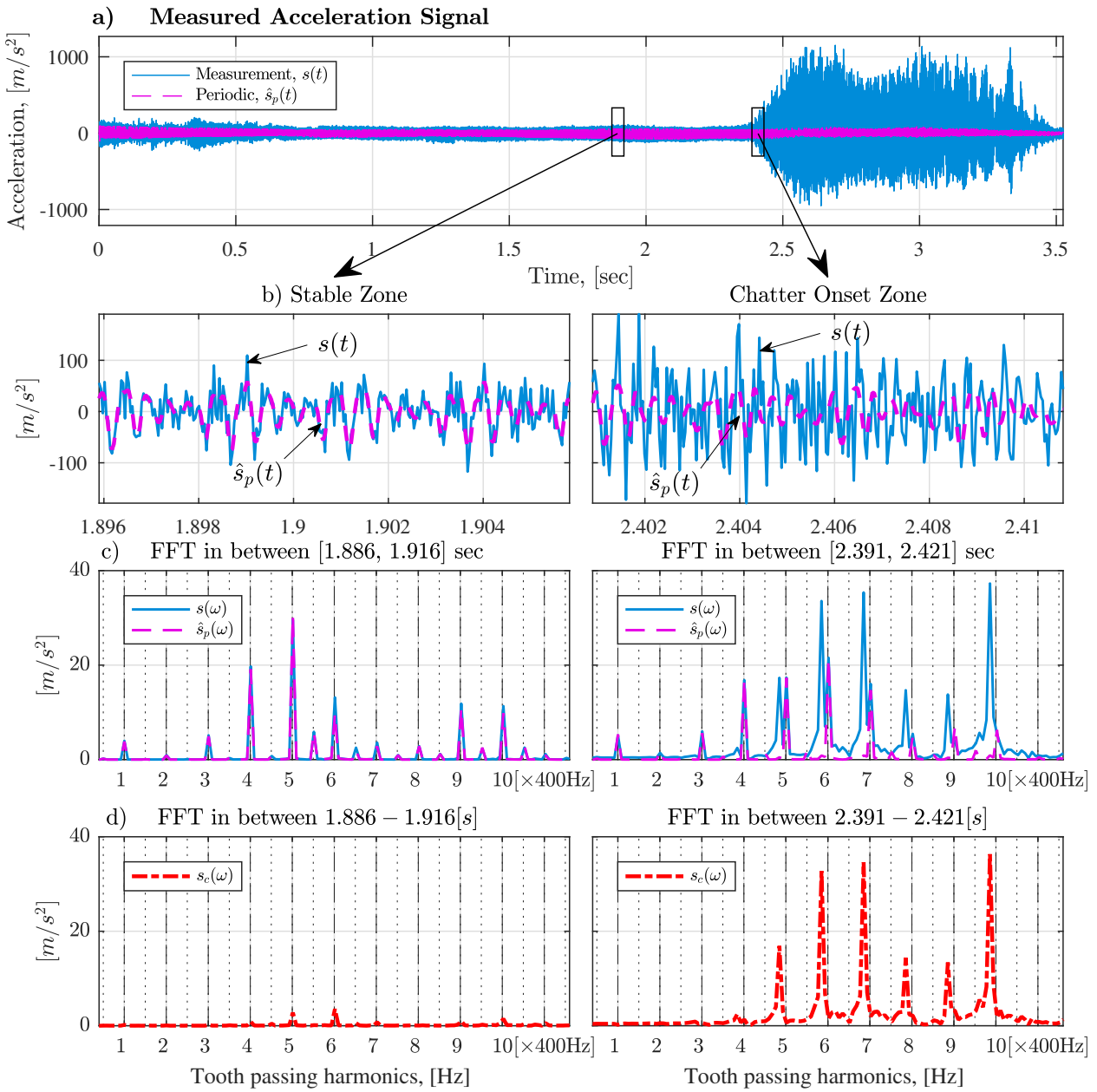

Fig. 5. Case 1: Separation of periodic and chatter components of measured acceleration signals. Cutting conditions: Tool diameter: 10 mm with 2 flutes, spindle speed: 12000 [rev/min], feed: 1800 [mm/min] (0.075 [mm/tooth]), axial depth of cut: 14 mm, the radial depth of cut increases linearly from 1.5 to 3 mm. Dashed lines show tooth passing frequency harmonics ($\omega_t = 400$ Hz) while the dotted lines show spindle frequency harmonics ($\omega_s = 200$ Hz).

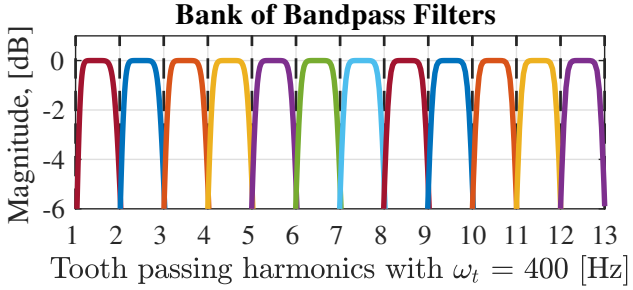

Fig. 6. Case 1: Bank of band-pass filters

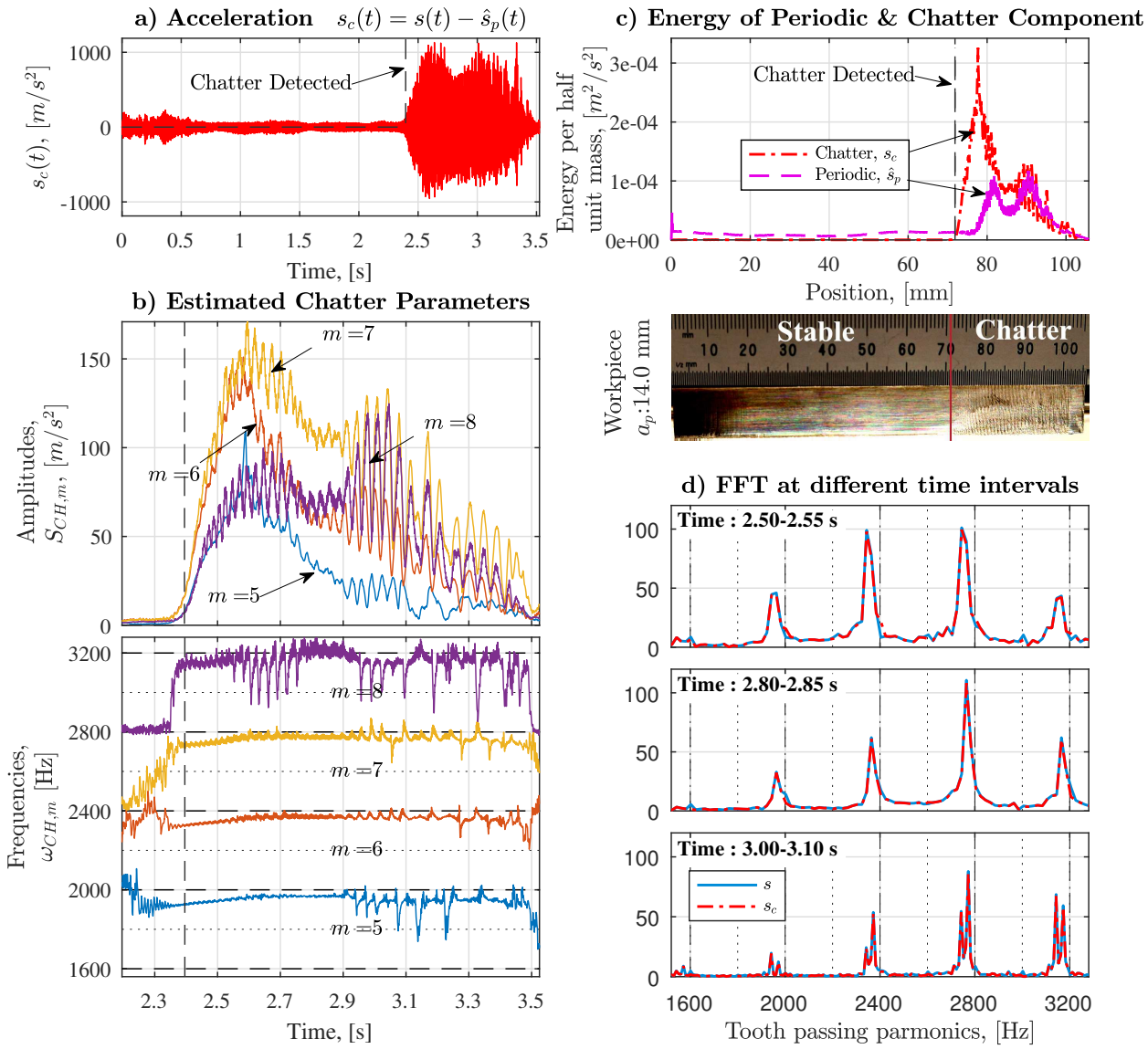

Fig. 7. Case 1: Chatter signals isolated from the measurements. Estimated chatter amplitudes $S_{c,m}$ and frequencies $\omega_{CH,m}$ from the chatter signal $s_c(t)$ for tooth passing harmonic intervals $m = 5,6,7,8$. FFTs are used to validate the algorithm. Cutting conditions are given in Fig. 5

chatter frequencies and amplitudes are validated by taking the power spectrum of the chatter signals at different time zones as shown in Fig. 7.d. At time $t = 2.8 - 2.85$[s], the chatter at $\omega_{CH,6} = 2769$ Hz becomes dominant due to changing radial depth of cut. Near the tool exit, around $t = 3.0 - 3.1$[s], the chatter vibrations become so heavy that the tool starts jumping out of cut exhibiting transient vibrations as well. This is also seen both at the amplitude graph and the third FFT spectrum. Moreover, the spectrum shows double peaks due to transient vibrations coupled with chatter.

Energy ratio as chatter indicator: The application of chatter detection algorithm is illustrated on the same experimental data as shown in Fig. 7.c. If the process is stable, the chatter component will not exist and the chatter energy will be close to zero as evident in Fig. 7.c. While the energy of the periodic-forced vibrations dominates at the stable zone (i.e., 0 to 72 mm distance along the tool path or 0 to 2.4[s] time interval), the chatter energy jumps significantly when the process becomes unstable. Tool starts leaving the cut after 80 mm distance, and energy values exhibit transient behavior which has to be disregarded. The measured acceleration and sound data from the same test are used to illustrate the chatter indicator in Fig. 8. The ratio of chatter energy over periodic-forced vibration energy (ER in Eq. (28)) jumps abruptly when the process becomes unstable, as seen in Fig. 8.b. Although the chatter detection threshold can be set to any value depending on the roughing or finishing applications, it is set to 20% in this case to account for noise and uncertainties in the measurements. When the cut is stable, the ER is always under the threshold limit. When the unstable cut starts, the indicator increases at the same time, and the energy ratio reaches to 90%.

Case 2: Milling a rigid aluminum workpiece with a 19.05 mm diameter, four fluted flexible end mill:

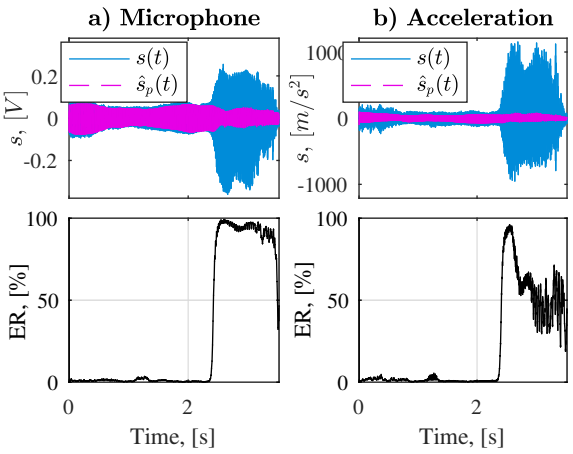

Fig. 8. Case 1: Comparison of microphone and acceleration for chatter detection. Cutting conditions are given in Fig. 5

The acceleration and sound data were collected at the sampling frequency of 10240 Hz. The measuremenst and processed signals are given in Fig. 9 along with the cutting conditions. Tool is flexible with the dominant vibration modes at 780 Hz, 825 Hz and 1143 Hz. The process was stable at the axial depth of 20 mm, but unstable at 25 mm depth of cut in down milling operations. The spindle speed was 10000 [rev/min] in both cases with a 0.953 mm constant radial depth of cut. Kalman filter is designed by considering $N = 20$ spindle harmonics, i.e., it covers frequency range up to $N\omega_s = 3330$ Hz. The $\lambda = Q/R$ gain between the process and measurement noise is set to 10^{-4}. The difference in λ value when compared to Case 1 ($\lambda = 10^{-6}$) is due to the lower sampling frequency, because increasing the sampling time increases the process noise. To isolate the chatter frequencies, $M = 4$ number of Butterworth 4-th order bandpass filters, covering the frequency range of $667 - 3330$ Hz, are used. In the stable test (Fig. 9.a) the cutting starts at $t = 0.02$[s]. The high ER during air cutting is due to missing periodic-forced vibrations. Right after cutting starts, Kalman filter estimates the periodic component, thus the ER decreases. The estimated frequencies either converge to the closest tooth passing harmonics, or fluctuate randomly at the stable cut. At time $0.1 - 0.2$[s] the frequency $\omega_{CH,2}$ has the highest amplitude but converges to the 5-th spindle harmonics at 830 Hz. FFT graphs shown in Fig. 9.d also exhibits the same behavior. Since this term belongs to forced vibrations, the energy of the chatter component is low (see Fig. 9.b). This is a typical resonance vibration case where the 5-th spindle harmonics excited one of the dominant vibration modes at 830 Hz. The process became unstable and chattered when the axial depth of cut was increased from 20 to 25 mm. Energy ratio (ER) graph shows that over 50% of the vibration energy is due to chatter. The estimated chatter frequency of $\omega_{CH,2} = 1200$ Hz is clearly seen from the frequency estimation and matches with the FFT results. The estimated amplitude of the signal between time $0.1 - 0.2$[s] is about 6 mV, which agrees with the FFT results.

Case 3: Comparison of microphone and accelerometer in chatter detection using energy ratio

A flexible tool (Sandvik R390-020-A20L holder with R390-11T308E-NL insert) with 20 mm diameter and 2 teeth has been used in milling a rigid aluminum Al7050-T7451 block. The two dominant tool vibration modes are at 732 Hz and 1180 Hz. Spindle vibrations have been collected with a Wilcoxon 786A accelerometer having 100[mV/g] sensitivity. Both accelerometer and microphone signals have been collected at 25600 Hz sampling frequency. The axial depth of cut was 0.8 mm and radial depth of cut was increased from 0 to 20 mm linearly along 150 mm tool path. The spindle speed was 9000 [rev/min]. Figure 10 shows the performance of energy ratio as chatter indicator for microphone and spindle acceleration signals. Kalman filter covers the frequency range up to 4.8 kHz ($N = 32$) and $M = 15$ number of bank of bandpass filters have been used to cover the frequency range of $300 - 4800$ Hz. The spindle speed and motor current set-point signals were collected at 10 kHz sampling frequency by TNC scope. This software runs on an external PC and communicates with the machines Heidenhain CNC via Ethernet. Although the ER amplitudes are different quantitatively for microphone and accelerometer due to different gains, their qualitative behavior are similar hence either can be used for chatter detection. The spindle speed and current signals performed well for detecting chatter. The energy ratio trends of these two signals are very similar, because the chatter frequency is higher than the bandwidth of the spindle speed and current controllers. In this high frequency region, the relation between the cutting force and spindle speed (as well as current) is determined by a simple integrator, i.e., $\omega(s)/T_d(s) \cong K_1/s$; $I_r(s)/T_d(s) \cong K_2/s$ where, ω is the spindle speed in rad/s, T_d is the disturbance motor torque in Nm, I_r is the current set-point in A, K_1 and K_2 are the DC gains determined by system parameters, s is the Laplace operator. Note that, in the energy calculation of the spindle speed and current measurements, the integration factor η in Eq. (28) is set as $\eta = 0$. This is due to the integrator behavior between motor torque and spindle speed (as well as current) transfer functions. Since the motor torque is generated by the cutting force and related to the acceleration of tool vibrations, spindle speed and current signals are treated as velocity type signals.

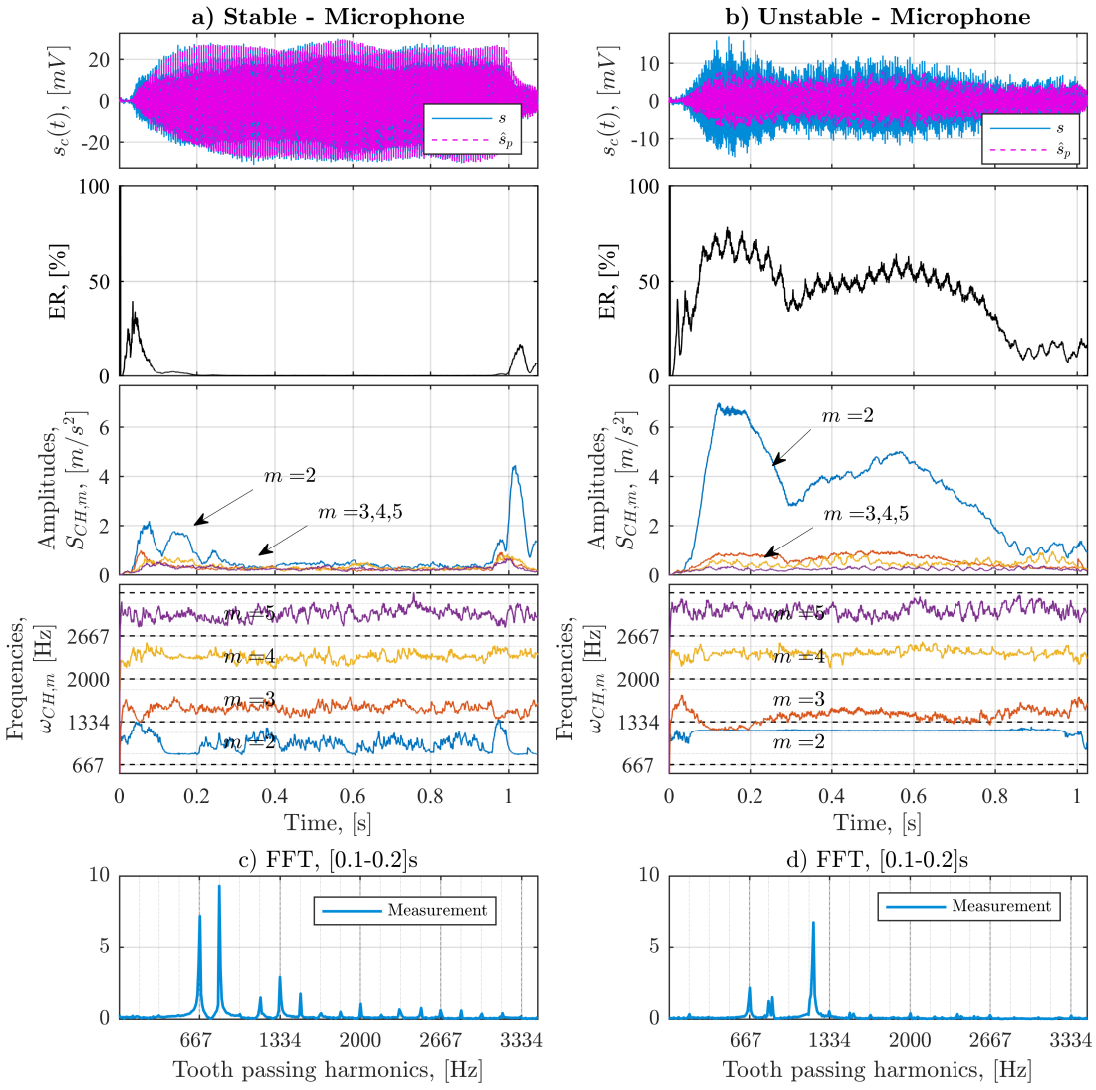

Fig. 9. Case 2: Measured microphone signals from stable and unstable milling experiments. Cutting conditions: Down milling of Aluminum AL7050-T7451, tool diameter: 19.05 mm with 4 flutes, spindle speeds: 10000 [rev/min], tooth passing frequency $\omega_t = 667$[Hz], feed: 10000 [mm/min] (0.250 [mm/tooth]). Radial depth of cut is 0.953 mm, axial depth of cut is 20 mm for the stable (a) and 25 mm for the unstable (b) cuts.

5 Conclusion

Detection of chatter and its frequency without false alarms is essential to achieve unattended, intelligent CNC machine tools. Once the presence of chatter and its frequency are detected, it is trivial to match the spindle speed with the sub-harmonics of chatter to convert the chatter into stable, forced vibrations. However, the key challenge is to separate the forced vibrations from chatter. Depending on the distribution of structural modes, cutting conditions, or tools having run-out or variable pitch, the amplitudes of forced vibrations may even be higher than regenerative terms despite the presence of chatter. This paper presents a discrete time, physics based on-line chatter detection strategy. The forced and self excited vibration frequencies are separated, and their energy ratio is monitored at each sampling time to detect the chatter and its frequency in a robust manner.

The mathematical model of milling system is formed as a combination of its forced and chatter vibration components. A Kalman filter is designed to estimate the periodic component of the measured signal and the amplitudes of its harmonics. The chatter component is extracted by subtracting the periodic part from the measured signal. The chatter frequency and amplitudes are estimated using Teager-Kaiser Nonlinear Energy Operator. Using the frequency and amplitude information, the energy of the periodic and chatter components are calculated at each sampling interval. The presence of chatter is detected by monitoring the energy ratio of the chatter component. The method has been tried on sound, acceleration, force, motor current set-point and spindle speed signals successfully. The chatter detection threshold is assigned considering the

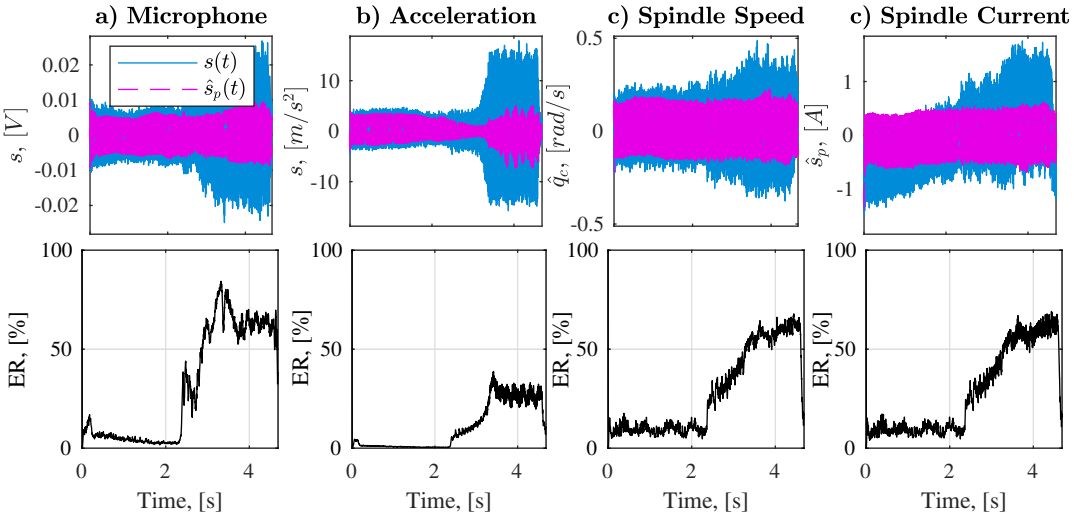

Fig. 10. Case 3: Comparison of microphone and acceleration signals, and spindle speed and motor current set-point signals with mean values removed. Cutting conditions: Down milling of Aluminum AL7050-T7451, tool diameter: 20 mm with 2 inserts, spindle speed: 9000 [rev/min], feed: 2000 [mm/min] (0.111 [mm/tooth]), axial depth of cut: 0.8 mm, the radial depth of cut increases from 0 to 20 mm linearly in 150 mm tool path.

uncertainties in the signal and numerical computation noise. Since sound and acceleration sensors are sufficient and most practical to be used in industry, their results are presented in the article. The proposed algorithm is integrated to our in-house developed intelligent machining system which includes adaptive control and tool failure detection as well.

Acknowledgements

This research is supported by the National Sciences and Engineering Research Council of Canada CANRIMT2 Strategic Research Network Grant (NETGP 479639-15) in machining. Dr. Hakan Caliskan is supported by The Scientific and Technological Research Council of Turkey, TUBITAK, with international postdoctoral fellowship program no 2219. Quaser machine tool is supplied by the CANRIMT2 partner ITRI (Taiwan), the cutters are supplied by the Sandvik Coromant.

References

[1] Y. Altintas, G. Stepan, D. Merdol, and Z. Dombovari. Chatter stability of milling in frequency and discrete time domain. CIRP Journal of Manufacturing Science and Technology, 1(1):35–44, 2008.

[2] T Delio, J Tlusty, and S Smith. Use of audio signals for chatter detection and control. ASME J. Eng. Ind, 114(2):146–157, 1992.

[3] E Kuljanic, Giovanni Totis, and Marco Sortino. Development of an intelligent multisensor chatter detection system in milling. Mechanical Systems and Signal Processing, 23(5):1704–1718, 2009.

[4] E Soliman and F Ismail. Chatter detection by monitoring spindle drive current. The International Journal of Advanced Manufacturing Technology, 13(1):27–34, 1997.

[5] M Lamraoui, Marc Thomas, and M El Badaoui. Cyclostationarity approach for monitoring chatter and tool wear in high speed milling. Mechanical Systems and Signal Processing, 44(1-2):177–198, 2014.

[6] Taejun Choi and Yung C Shin. On-line chatter detection using wavelet-based parameter estimation. Journal of manufacturing science and engineering, 125(1):21–28, 2003.

[7] I. N. Tansel, X Wang, P Chen, A Yenilmez, and B Ozcelik. Transformations in machining. part 2. evaluation of machining quality and detection of chatter in turning by using s-transformation. International Journal of Machine Tools and Manufacture, 46(1):43–50, 2006.

[8] Lei Wang and Ming Liang. Chatter detection based on probability distribution of wavelet modulus maxima. Robotics and Computer-Integrated Manufacturing, 25(6):989–998, 2009.

[9] Hongrui Cao, Yaguo Lei, and Zhengjia He. Chatter identification in end milling process using wavelet packets and hilbert–huang transform. International Journal of Machine Tools and Manufacture, 69:11–19, 2013.

[10] Janez Gradišek, Edvard Govekar, and Igor Grabec. Using coarse-grained entropy rate to detect chatter in cutting. Journal of sound and vibration, 214(5):941–952, 1998.

[11] Daniel Perez-Canales, Luciano Vela-Martínez, Juan Carlos Jáuregui-Correa, and Jose Alvarez-Ramirez. Analysis of the entropy randomness index for machining chatter detection. International Journal of Machine Tools and Manufacture, 62:39–45, 2012.

[12] Yang Fu, Yun Zhang, Huamin Zhou, Dequn Li, Hongqi Liu, Haiyu Qiao, and Xiaoqiang Wang. Timely online chatter detection in end milling process. Mechanical Systems and Signal Processing, 75:668–688, 2016.

[13] Yongjian Ji, Xibin Wang, Zhibing Liu, Zhenghu Yan, Li Jiao, Dongqian Wang, and Junqing Wang. Eemd-based online milling chatter detection by fractal dimension and power spectral entropy. The International Journal of Advanced Manufacturing Technology, pages 1–16, 2017.

[14] Hongrui Cao, Kai Zhou, and Xuefeng Chen. Chatter identification in end milling process based on eemd and nonlinear dimensionless indicators. International Journal of Machine Tools and Manufacture, 92:52–59, 2015.

[15] N. J. M. Van Dijk, E. J. J. Doppenberg, R. P. H. Faassen, N Van De Wouw, J. A. J. Oosterling, and H Nijmeijer. Automatic in-process chatter avoidance in the high-speed milling process. Journal of dynamic systems, measurement, and control, 132(3):031006, 2010.

[16] E Kuljanic, Marco Sortino, and G Totis. Multisensor approaches for chatter detection in milling. Journal of Sound and Vibration, 312(4):672–693, 2008.

[17] X. Q. Li, Y. S. Wong, and A. Y. C. Nee. Tool wear and chatter detection using the coherence function of two crossed accelerations. International Journal of Machine Tools and Manufacture, 37(4):425–435, 1997.

[18] Katja M Hynynen, Juho Ratava, Tuomo Lindh, Mikko Rikkonen, Ville Ryynänen, Mika Lohtander, and Juha Varis. Chatter detection in turning processes using coherence of acceleration and audio signals. Journal of Manufacturing Science and Engineering, 136(4):044503, 2014.

[19] S Tangjitsitcharoen and T Moriwaki. Intelligent identification of turning process based on pattern recognition of cutting states. Journal of materials processing technology, 192:491–496, 2007.

[20] Tony L Schmitz. Chatter recognition by a statistical evaluation of the synchronously sampled audio signal. Journal of Sound and Vibration, 262(3):721–730, 2003.

[21] Tamás Insperger, Brian P Mann, Tobias Surmann, and Gábor Stépán. On the chatter frequencies of milling processes with runout. International Journal of Machine Tools and Manufacture, 48(10):1081–1089, 2008.

[22] Yasuhiro Kakinuma, Yui Sudo, and Tojiro Aoyama. Detection of chatter vibration in end milling applying disturbance observer. CIRP Annals-Manufacturing Technology, 60(1):109–112, 2011.

[23] Emad Al-Regib and Jun Ni. Chatter detection in machining using nonlinear energy operator. Journal of dynamic systems, measurement, and control, 132(3):034502, 2010.

[24] Y Altintas and Philip K Chan. In-process detection and suppression of chatter in milling. International Journal of Machine Tools and Manufacture, 32(3):329–347, 1992.

[25] Adly A Girgis, W Bin Chang, and Elham B Makram. A digital recursive measurement scheme for online tracking of power system harmonics. IEEE transactions on Power Delivery, 6(3):1153–1160, 1991.

[26] E. Budak and Y. Altintas. Analytical prediction of chatter stability in millingpart i: general formulation. Journal of dynamic systems, measurement, and control, 120(1):22–30, 1998.

[27] Yusuf Altintas. Manufacturing automation: metal cutting mechanics, machine tool vibrations, and CNC design. Cambridge university press, 2012.

[28] J-J Junz Wang, Steven Y Liang, and Wayne John Book. Convolution analysis of milling force pulsation. Journal of Engineering for Industry, 116(1):17–25, 1994.

[29] Li Zheng, Steven Y Liang, and Shreyes N Melkote. Angle domain analytical model for end milling forces. Journal of manufacturing science and engineering, 120(2):252–258, 1998.

[30] C Eksioglu, Z. M. Kilic, and Y Altintas. Discrete-time prediction of chatter stability, cutting forces, and surface location errors in flexible milling systems. Journal of Manufacturing Science and Engineering, 134(6):061006, 2012.

[31] Tamás Insperger, Gábor Stépán, PV Bayly, and BP Mann. Multiple chatter frequencies in milling processes. Journal of sound and vibration, 262(2):333–345, 2003.

[32] Robert Grover Brown and Patrick Y. C. Hwang. Introduction to Random Signals and Applied Kalman Filtering with Matlab-4th Ed. Wiley, -, 2012.

[33] James F Kaiser. On a simple algorithm to calculate the'energy'of a signal. In Acoustics, Speech, and Signal Processing, 1990. ICASSP-90., 1990 International Conference on, pages 381–384. IEEE, 1990.

[34] Petros Maragos, James F Kaiser, and Thomas F Quatieri. Energy separation in signal modulations with application to speech analysis. IEEE transactions on signal processing, 41(10):3024–3051, 1993.

[35] Wei Lin, Chris Hamilton, and Prabhakar Chitrapu. A generalization to the teager-kaiser energy function and application to resolving two closely-spaced tones. In Acoustics, Speech, and Signal Processing, 1995. ICASSP-95., 1995 International Conference on, volume 3, pages 1637–1640. IEEE, 1995.

[36] Samir N. Y. Gerges, G. A. Sehrndt, and W Parthey. Noise sources. Occupational exposure to noise: Evaluation, prevention and control. Publication Series from the Federal Institute for Occupational Safety and Health. World Health Organization, 2001.

Appendix A: State Space Representation of Harmonic Signals

Consider a single frequency and noise free-signal as follows

$$x(t_k) = A(t_k)\cos(\omega t_k + \phi) \tag{30}$$

where $t_k = kT$ is the time at time step k with sampling period T. Let the first state be $q_{1,k} = x_k$, and at time $t_{k+1} = t_k + T$ it is expressed as:

$$\begin{aligned} q_{1,k+1} &= A_{k+1}\cos\left(\omega(t_k+T)+\phi\right) = x_{k+1} \\ &= A_{k+1}\left[\cos(\omega t_k+\phi)\cos(\omega T) - \sin(\omega t_k+\phi)\sin(\omega T)\right] \end{aligned} \tag{31}$$

By selecting the second state as $q_{2,k} = A_k \sin(\omega t_k + \phi)$ and expressing it at time t_{k+1}:

$$\begin{aligned} q_{2,k+1} &= A_{k+1}\sin(\omega t_{k+1}+\phi) \\ &= A_{k+1}\left[\cos(\omega t_k+\phi)\sin(\omega T) + \sin(\omega t_k+\phi)\cos(\omega T)\right] \end{aligned} \tag{32}$$

The state variable representation of the signal Eq. (30) becomes:

$$\underbrace{\begin{bmatrix} q_{1,k+1} \\ q_{2,k+1} \end{bmatrix}}_{\mathbf{q}_{k+1}} = \underbrace{\begin{bmatrix} \cos(\omega T) & -\sin(\omega T) \\ \sin(\omega T) & \cos(\omega T) \end{bmatrix}}_{\Phi} \underbrace{\begin{bmatrix} q_{1,k} \\ q_{2,k} \end{bmatrix}}_{\mathbf{q}_k} + \underbrace{\begin{bmatrix} w_{1,k} \\ w_{2,k} \end{bmatrix}}_{\mathbf{w_k}} \tag{33}$$

where $\mathbf{w}_k$ is the process noise and accounts for the time variation of the amplitude and phase. Noting the first state is selected as the measured signal, i.e., $q_{1,k} = s_k$, the measurement equation with the signal and measurement noise, v_k becomes:

$$z_k = \underbrace{\begin{bmatrix} 1 & 0 \end{bmatrix}}_{\mathbf{H}} \begin{bmatrix} q_{1,k} \\ q_{2,k} \end{bmatrix} + v_k \tag{34}$$

Appendix B: Estimation of vibration frequency and amplitude from energy in discrete time domain

Kaiser introduced [33] Teager's algorithm for estimating a measure of energy in a single component signal. The proposed energy operator is based on the following undamped single degree of freedom system:

$$m\ddot{x} + kx = 0 \tag{35}$$

whose solution is a harmonic motion oscillating at natural frequency $\omega = \sqrt{k/m}$ with amplitude A and phase angle ϕ:

$$x(t) = A\cos(\omega t + \phi) \tag{36}$$

By substituting $kx = -m\ddot{x}$,the total kinetic and potential energy ($E(t)$) of the oscillating system is,

$$E(t) = \frac{1}{2}m\left[\dot{x}(t)\right]^2 + \frac{1}{2}k\left[x(t)\right]^2 = \frac{m}{2}A^2\omega^2 \tag{37}$$

The following continuous Teager-Kaiser Nonlinear Energy Operator (NEO) is introduced as a measure of the energy per half unit mass as for the displacement $\Psi_c\left[x(t)\right]$ and velocity $\Psi_c\left[\dot{x}(t)\right]$ as [34]

$$\left.\begin{aligned}\Psi_c\left[x(t)\right] &= \dot{x}(t)^2 - x(t)\ddot{x}(t) = A^2\omega^2 \\ \Psi_c\left[\dot{x}(t)\right] &= \ddot{x}(t)^2 - \dot{x}(t)\dddot{x}(t) = A^2\omega^4\end{aligned}\right\} \tag{38}$$

Maragos et. al. [34] introduced the application of energy operator to the estimation of the frequency and amplitude of the vibrations in the continuous time domain data as :

$$\omega = \sqrt{\frac{\Psi_c\left[\dot{x}(t)\right]}{\Psi_c\left[x(t)\right]}} \qquad |A| = \frac{\Psi_c\left[x(t)\right]}{\sqrt{\Psi_c\left[\dot{x}(t)\right]}} \tag{39}$$

Discrete time equivalent of NEO is evaluated by approximating the derivatives with Euler backward difference method. By introducing $t_k = kT$, $\theta = \omega T$, $y(t_k) = x(t_k) - x(t_{k-1})$, the displacement and its derivatives at T[s] sampling intervals become [34]:

$$\left.\begin{aligned}x(t_k) &= A\cos(\omega kT + \phi) \\ &= A\cos(k\theta + \phi) \qquad k = 0, 1, 2, 3, ... \\ \dot{x}(t_k) &= \frac{x_k - x_{k-1}}{T} = \frac{y_k}{T} \\ y(t_k) &= -2A\sin\left(\frac{\theta}{2}\right)\sin\left(k\theta - \frac{\theta}{2} + \phi\right) \\ \ddot{x}(t_k) &= \frac{y_k - y_{k-1}}{T^2}\end{aligned}\right\} \tag{40}$$

Discrete equivalent of NEO becomes:

$$\left.\begin{aligned}\Psi\left[x(t_k)\right] &= \frac{1}{T^2}\left(x_{k-1}^2 - x_k x_{k-2}\right) \\ &= \frac{A^2}{T^2}\sin^2\theta \\ &= A^2\omega^2\left(\frac{\sin\theta}{\theta}\right)^2 \\ \Psi\left[y(t_k)\right] &= \frac{4A^2}{T^2}\sin^2\left(\frac{\theta}{2}\right)\sin^2\left(\theta\right)\end{aligned}\right\} \tag{41}$$

The operator θ can be evaluated as:

$$\frac{\Psi\left[y(t_k)\right]}{2\Psi\left[x(t_k)\right]} = 2\sin^2\left(\frac{\theta}{2}\right) = 1 - \cos\left(\theta\right) \tag{42}$$

By averaging two consecutive NEOs, the corresponding frequency $\omega(k)$ and amplitude at each sampling interval k can be found as :

$$\left.\begin{aligned}\theta(t_k) &= \arccos\left(1 - \frac{\Psi_d[y_k] + \Psi_d[y_{k+1}]}{4\Psi_d[x_k]}\right) \\ \omega(t_k) &= \theta_k / T \\ |\,A_{t_k}\,| &= \sqrt{\frac{\Psi_d[x_k]}{1 - \left(1 - \frac{\Psi_d[y_k] + \Psi_d[y_{k+1}]}{4\Psi_d[x_k]}\right)^2}}\end{aligned}\right\} \tag{43}$$

Further details of the method can be found in [34].